Galactic Dynamics in the Era of Large Surveys
Proceedings IAU Symposium No. 353, 2019
M. Valluri & J. A. Sellwood, eds.

doi:10.1017/S1743921319008640

New structures of the Milky Way stellar and dark halos revealed from the Subaru/Hyper Suprime-Cam survey

Masashi Chiba

Astronomical Institute, Tohoku University, Sendai 980-8578, Japan
email: chiba@astr.tohoku.ac.jp

Abstract. We present the recent discovery of new halo structures in the Milky Way (MW) based on the Hyper Suprime-Cam (HSC) Subaru Strategic Program (SSP). HSC is a wide-field imager installed at the prime focus of the Subaru Telescope, and a 300-night survey with this instrument is being carried out in this program. The combination of the superb image quality and depth and the fact that it is a multi-band survey allows us to identify new faint satellites as well as field halo stars in the outskirts of the MW halo beyond the reach of previous surveys. We report here on the new insights into the nature of both stellar and dark halos in the MW as revealed from this on-going survey program and show prospects based on the upcoming large spectroscopic survey with Subaru Prime Focus Spectrograph.

Keywords. Galaxy: halo, formation, cosmology: dark matter

1. Introduction

The currently standard cosmological model based on Λ-dominated cold dark matter (ΛCDM) predicts that objects in the Universe grow hierarchically; they become progressively more massive with time through accretion and mergers. This model reproduces the observed cosmic large-scale structure on scales $\gtrsim 1$ Mpc extremely well (e.g., Tegmark *et al.* 2004). The model also provides a standard theory for understanding the formation and evolution of galaxies based on hierarchical assembly of smaller stellar systems such as dwarf galaxies. However, this standard model suffers from several tensions on smaller scales, including the missing satellites problem (Klypin *et al.* 1999; Moore *et al.* 1999), namely that a Milky Way sized halo is predicted to have significantly more subhalos than the observed number of dwarf satellites. Also, the detailed assembly process in the formation of galactic structures is not fully understood yet, especially for our home, the Milky Way (MW).

The key information in all of these issues is imprinted in the halo of the MW. Indeed, regarding the missing satellites problem, it is suggested that our catalogs of dwarf satellites in the MW halo are yet incomplete owing to observational constraints such as limited survey area and depth. However, the observational situation has dramatically improved in recent years thanks largely to modern massive imaging surveys, including the Sloan Digital Sky Survey (SDSS) and the Dark Energy Survey (DES). Such systematic surveys over the halo of the MW are also providing several basic properties of its stellar components that contain the relics of galaxy formation in terms of global density structures and streams/substructures. Thus, the MW halo is indeed an excellent probe for the nature of dark matter and galaxy formation.

For these scientific objectives, we are now conducting an extensive search and analysis of new MW satellites as well as MW halo stars using data from the Hyper Suprime-Cam

Subaru Strategic Program (HSC-SSP) (Aihara *et al.* 2018). HSC is a wide-field imager installed at the prime focus of the Subaru Telescope, and a 300-night survey with this instrument is being carried out. In this contribution, we report the discovery of new ultra-faint dwarfs (UFDs) in the outer parts of the MW halo and the global density distribution of blue horizontal-branch stars (BHBs) as a tracer of the MW stellar halo. The detailed descriptions of these studies have been presented in Homma *et al.* (2018, 2019) and Fukushima *et al.* (2019), respectively.

2. New Milky Way Satellites

We use the g, r, and i-band data obtained from internal data release S18A of HSC-SSP, which covers, in its Wide layer, ~ 676 deg^2 in six separate fields along the celestial equator and one field around $(\alpha_{2000}, \delta_{2000}) = (242°, 43°)$.

For the search of new MW satellites, we first select stars that satisfy the following criteria: (1) their images are point-like to avoid galaxies, (2) their $g-r$ colors are bluer than 1 to eliminate foreground M-type main sequence disk stars, and (3) their $g-r$ vs. $r-i$ colors follow the fiducial relation expected for stars to remove remaining contaminants. Then, we search for statistically significant spatial overdensities of stars relative to the foreground and background noise from MW stars and distant galaxies/quasars. We look for overdensities using the color-magnitude (CMD) isochrone-based matched filter based on a PARSEC isochrone (Bressan *et al.* 2012), with which we set four different models: (a) an age of $t = 13$ Gyr and metallicity of [M/H]$= -1.5$, (b) $t = 13$ Gyr and [M/H]$= -2.2$, (c) $t = 8$ Gyr and [M/H]$= -1.5$, and (d) $t = 8$ Gyr and [M/H]$= -2.2$. After selecting stars using the above isochrone filters at each distance, we search for spatial overdensities and examine their statistical significance. We count selected stars in $0°.05 \times 0°.05$ bins in right ascension and declination, with an overlap of $0°.025$ in each direction.

Using the algorithm above, we have found four new overdensities with high statistical significance, all of which have been found through the isochrone filter of $t = 13$ Gyr and [M/H]$= -2.2$ (Figure 1). These are named as Virgo I, Cetus III, Boötes IV and HSC 1, and the basic structural properties of these systems are summarized in Table 1.

To compare these stellar systems with known MW globular clusters and dwarf satellites. we show, in Figure 2(a), the relation between the half-light radii, r_h, and V-band absolute magnitudes, M_V, of globular clusters in the MW (dots) and those of dwarf satellites (squares). Stars in this diagram denote the currently identified new stellar systems. It is clear that Virgo I, Cetus III and Boötes IV are significantly large compared with MW globular clusters having similar M_V and that they follow the locus of MW dwarf satellites. This suggests that these are typical UFDs. On the other hand, the size of HSC 1 is comparable to MW globular clusters, although it is still possible that it is a compact dwarf galaxy because HSC 1 lies on the M_V vs. r_h relation for dwarf galaxies.

Figure 2(b) presents the relation between M_V and heliocentric distance $D_\odot$ for all the objects shown in Figure 2(a). Also shown are the detection limits of SDSS and HSC, suggesting that the newly found stellar systems are beyond the reach of SDSS.

We have discovered, at least, three new dwarf satellites from the HSC-SSP data released internally in the outer halo of the MW. In addition, there are three known satellites within the HSC-SSP footprint: Sextans ($M_V = -9.3$: classical dwarf), Leo IV ($M_V = -5.8$: SDSS DR9) and Pegasus III ($M_V = -3.4$: SDSS DR9), so that there are six satellites over the area of ~ 676 deg^2.

To compare this discovery rate with the prediction of ΛCDM models, we adopt the two recent works by Newton *et al.* (2018) and Dooley *et al.* (2017) for the number of visible satellites expected in ΛCDM models. Newton *et al.* (2018) combined the data from SDSS and DES surveys to infer the full complement of MW satellite galaxies. For this purpose, they adopted the subhalo populations for MW-sized halos performed by

https://doi.org/10.1017/S1743921319008640 Published online by Cambridge University Press

Table 1. Properties of new stellar systems found in HSC footprints.

Parameter	Virgo I	Cetus III	Boötes IV	HSC 1
Coordinates (J2000)	180°.038, −0°.681	31°.331, −4°.270	233°.689, 43°.726	334°.309, 3°.480
Galactic Coordinates (l, b)	276°.942, +59°.578	163°.810, −61°.133	70°.682, 53°.305	66°.319, −41°.841
Position angle (deg)	$+62^{+8}_{-13}$	$+101^{+5}_{-6}$	$+3^{+4}_{-4}$	-12^{+11}_{-11}
Ellipticity	$0.59^{+0.12}_{-0.14}$	$0.76^{+0.06}_{-0.08}$	$0.64^{+0.05}_{-0.05}$	$0.46^{+0.08}_{-0.10}$
Number of stars, N_*	18^{+5}_{-4}	16^{+3}_{-5}	124^{+10}_{-10}	47^{+6}_{-6}
Extinction, A_V (mag)	0.066	0.066	0.067	0.222
$(m-M)_0$ (mag)	$19.8^{+0.2}_{-0.1}$	$22.0^{+0.2}_{-0.1}$	$21.6^{+0.2}_{-0.2}$	$18.3^{+0.2}_{-0.2}$
Heliocentric distance (kpc)	91^{+9}_{-4}	251^{+24}_{-11}	209^{+20}_{-18}	46^{+4}_{-4}
Half light radius, r_h (pc)	47^{+19}_{-13}	90^{+42}_{-17}	462^{+98}_{-84}	$5.9^{+1.5}_{-1.3}$
$M_{\mathrm{tot},V}$ (mag)	$-0.33^{+0.75}_{-0.87}$	$-2.45^{+0.57}_{-0.56}$	$-4.53^{+0.23}_{-0.21}$	$-0.20^{+0.59}_{-0.83}$

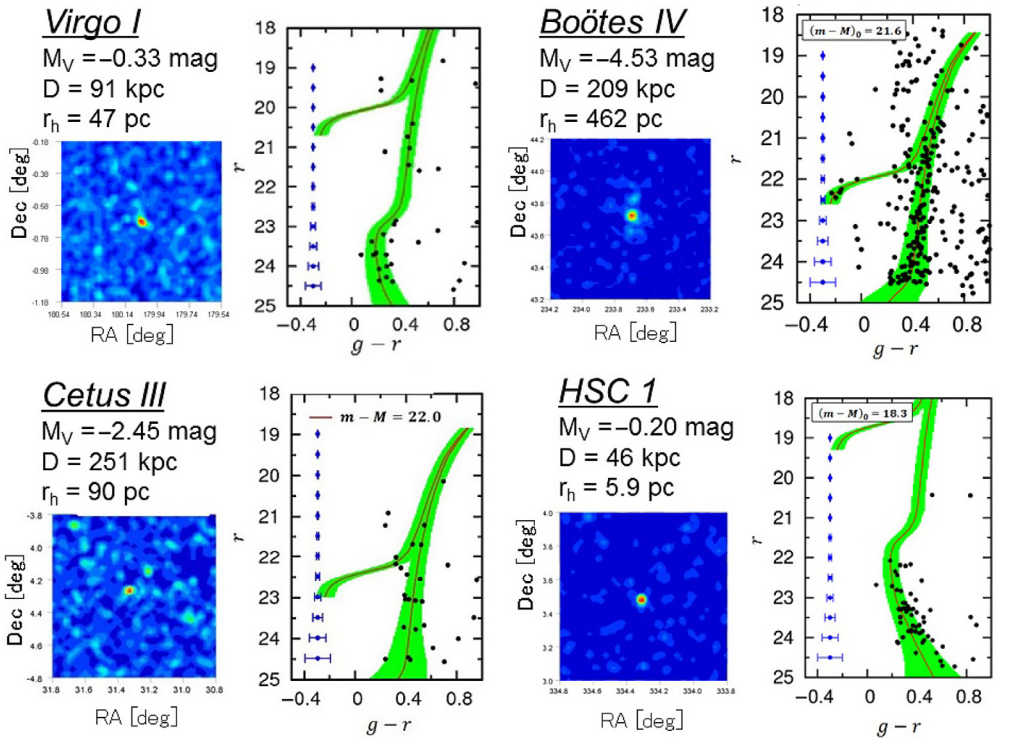

Figure 1. The stellar overdensities for the point sources (left) passing the isochrone filter of $t = 13$ Gyr and [M/H]$= -2.2$ at respective distances (right) for Virgo I, Cetus III, Boötes IV and HSC 1.

the simulation project, AQUARIUS (Springel *et al.* 2008). They obtained a prior for the radial distribution of satellites, which is modeled in terms of an Einasto profile (Einasto 1965). For an assumed MW halo mass of $1.0 \times 10^{12}\ M_\odot$, they found that the total number of satellites with $M_V \leqslant 0$ within 300 kpc of the Sun is 124^{+40}_{-27} (see their Table E1); this number is only weakly dependent on host halo mass. On the other hand, Dooley *et al.* (2017) considered the abundance matching method and the adopted radial distribution of satellites is less centrally concentrated than an Einasto or NFW profile, leading to the total number of satellites as many as 1000 for $M_V \leqslant 0$.

Given these predicted numbers of visible satellites, we evaluate the HSC-SSP survey area and depth to obtain the actual number of satellites it should be able to detect. First,

https://doi.org/10.1017/S1743921319008640 Published online by Cambridge University Press

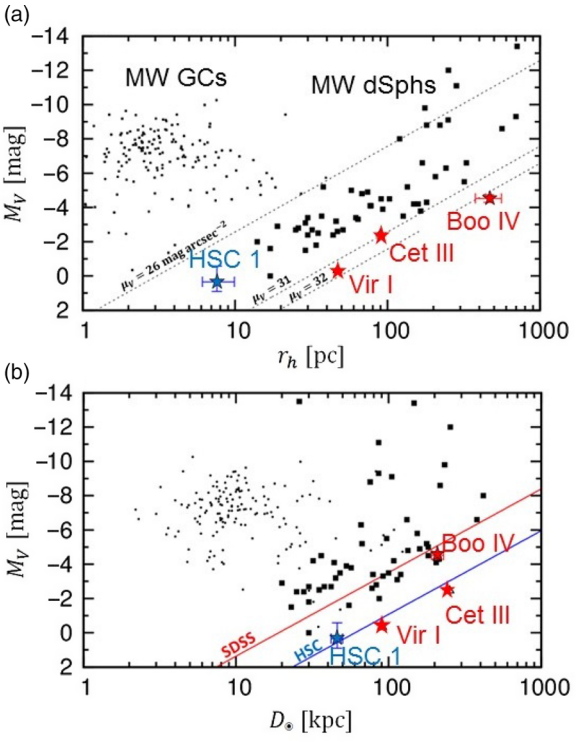

Figure 2. (a) The relation between M_V and r_h for MW globular clusters (dots) and MW dSphs (filled squares) The stars denote Virgo I, Cetus III, Boötes IV and HSC 1. The dotted lines denote the loci of constant surface brightness, $\mu_V = 26$, 31, and 32 mag arcsec^{-2}. (b) The relation between M_V and heliocentric distance, $D_\odot$.

HSC-SSP in its Wide layer has surveyed over ~ 676 deg^2, which corresponds to a fraction of the sky as 0.016. Second, we consider the completeness correction associated with the detection limit of HSC, which depends on M_V and the assumed radial distribution of satellites. Taking into account these two correction factors, the expected numbers of visible satellites in the HSC-SSP survey of S18A for $M_V \leqslant 0$ are given in the ranges of $1-2$ and $6-12$ based on Newton *et al.* (2018) and Dooley *et al.* (2017), respectively.

This suggests that if we adopt Newton *et al.* (2018), we apparently have a problem of too many satellites, instead of a missing satellites problem, whereas the prediction by Dooley *et al.* (2017) is roughly in agreement with the observed number of satellites. We note that this difference mainly originates from the adopted radial distribution of satellites after their completeness correction, as discussed in Kim *et al.* (2018). Indeed, the completeness correction is mostly determined by the satellites in the inner parts of the MW halo, not those far from the Sun such as those detected with Subaru/HSC.

As a conclusion, the missing satellites problem is perhaps not so serious compared with previously thought. For the more realistic estimate of the number of MW satellites, we suggest that deep surveys such as HSC-SSP and LSST are important to constrain the radial distribution of satellites in the outer parts of the halo.

3. Mapping the Milky Way Stellar Halo

For the purpose of mapping the MW stellar halo through the selection of blue-horizontal branch stars (BHBs), we adopt the g, r, i and z-band data from internal data

https://doi.org/10.1017/S1743921319008640 Published online by Cambridge University Press

release S18A of the Wide layer of HSC-SSP. The total area that the current data set covers is ~ 550 deg^2, among which we exclude the fields called GAMA15H and XMM-LSS because of the presence of several spatial substructures associated with the Sagittarius (Sgr) stream, This is because our interest here is to deduce the structure of the smooth halo component.

We first choose point sources with $i \leqslant 24.5$, for which the contamination of faint galaxies is estimated as $\sim 50\%$. Then, for the selection of BHBs, we confine ourselves to point sources in the following magnitude and color ranges: $18.5 < g < 23.5$, $-0.3 < g - r < 0$, $-0.4 < r - i < 0.4$ and $-0.25 < i - z < 0.1$, where the faint limit for the g-band magnitude range is taken based on its photometric error of typically $\simeq 0.05$ mag with maximum of $\simeq 0.1$ mag. These data contain not only BHBs but also other point sources such as blue straggler stars (BSs), white dwarfs (WDs), QSOs as well as faint galaxies. BHBs are distributed in the distinct region in the $i - z$ vs. $g - r$ diagram, because the $i - z$ color is affected by the Paschen features of stellar spectra and is sensitive to surface gravity (Lenz *et al.* 1998; Vickers *et al.* 2012; Fukushima *et al.* 2018). Thus, other A-type stars having higher surface gravity, i.e. BSs as well as WDs, can be excluded based on their distributions in the $i - z$ vs. $g - r$ diagram. Since QSOs are largely overlapping with BHBs in this diagram, the removal of these point sources also requires the use of the $g - z$ vs. $g - r$ diagram. In this work, as detailed in Fukushima *et al.* (2019), we adopt an extensive Bayesian method for the selection of BHB stars, given the likely distribution for each of the contaminants in the color-color diagrams defined by g, r, i and z-band.

For the distance estimates of BHBs, we adopt the formula for their g-band absolute magnitudes, $M_g^{\rm BHB}$, calibrated by Deason *et al.* (2011). We then derive the three dimensional positions of BHBs in rectangular coordinates, (x, y, z), for the Milky Way space, where the Sun is assumed to be at (8.5,0,0) kpc. Then, for the density distributions of BHBs, we adopt the following five models and apply the Goodman & Weare's Affine Invariant Markov chain Monte Carlo (MCMC) to estimate the associated parameters: spherical single power-law (SSPL), spherical broken power-law (SBPL), axially symmetric single power-law (ASPL), axially symmetric broken power-law (ABPL) and the Einast profile (Einasto 1965).

We find that ABPL model is most likely for reproducing the distribution of BHBs among the given models. This model is given as

$$\rho_{\rm halo}(r_q) \propto \begin{cases} r_q^{-\alpha_{\rm in}} & r_q \leqslant r_b \\ r_q^{-\alpha_{\rm out}} & r_q > r_b \end{cases} \tag{3.1}$$

where $r_q^2 = x^2 + y^2 + z^2 q^{-2}$ and q is the axis ratio. Here $\alpha_{\rm in}$ and $\alpha_{\rm out}$ denote the power-law indices in inner and outer halo regions, respectively, divided at the broken radius, r_b. We obtain $\alpha_{\rm in} = 2.92^{+0.33}_{-0.33}$, $\alpha_{\rm out} = 15.0^{+3.7}_{-4.5}$, $r_{\rm b}/{\rm kpc} = 160^{+18}_{-19}$ and $q = 1.72^{+0.44}_{-0.28}$. This suggests that this halo may hold a rather sharp boundary at $r_{\rm b} \sim 160$ kpc.

For the comparison with other previous surveys for tracing the MW stellar halo, we note that except for the following recent work, most of the other surveys are devoted to the halo regions at Galactocentric radii well below $r = 100$ kpc (see Figure 3 showing various survey results). Recently, Thomas *et al.* (2018) combined their CFIS survey made in deep u-band with $griz$-band data from Pan-STARRS 1 to select candidate BHBs. Their analysis revealed that a broken power-law model with an inner/outer slope of 4.24/3.21 at a break radius of 41.4 kpc is the best fitting case out to $r \sim 220$ kpc. This outer slope is similar to the inner slope of $\simeq 2.92$ in our ABPL model at $r < r_{\rm b} \simeq 160$ kpc, thus giving an approximate agreement.

The surveys using RR Lyrae at r as large as 100 kpc tend to provide different density slopes (Watkins *et al.* 2009; Cohen *et al.* 2017; Hernitschek *et al.* 2018). These works show $\alpha = 4.0 \sim 4.5$ at $r > 25$ kpc, which is systematically steeper than the slopes obtained

https://doi.org/10.1017/S1743921319008640 Published online by Cambridge University Press

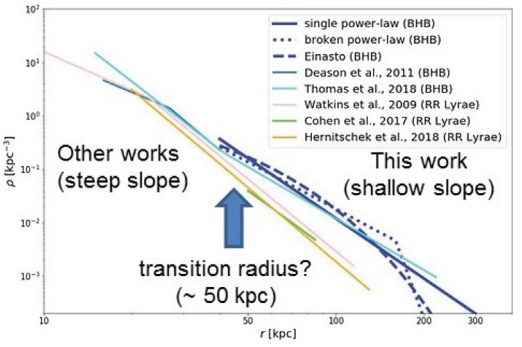

Figure 3. Comparison of our best-fit models, the single power-law (blue solid line), broken power-law (blue dotted line), and the Einasto profile (blue dashed line), with other works using BHBs (Deason *et al.* 2011; Thomas *et al.* 2018) and RR Lyrae (Watkins *et al.* 2009; Cohen *et al.* 2017; Hernitschek *et al.* 2018).

here for BHBs, but consistent with those for BSs located at similar radii to RR Lyrae ($\alpha \simeq 4.50$ for ASPL, $\alpha_{\rm out} \simeq 4.22$ for ABPL). This implies that the difference in the value of the density slope for BHBs from that for RR Lyrae is due to the difference in the range of Galactocentric radii for the adopted sample. Another possible reason for the different slopes may be due to the intrinsically different radial distribution for a different stellar sample, depending on the formation history of a stellar halo associated with merging/accretion of progenitor dwarf galaxies.

To infer what constraints from the current analysis of BHBs can be made on the past accretion history of the MW halo, we compare with the suite of hydrodynamical simulations for galaxy formation by Rodriguez-Gomez *et al.* (2016) using the Illustris Project. They investigated the formation of galaxies over a wide range of stellar masses, $M_* = 10^9 - 10^{12} M_\odot$, and obtained the relative contribution of the so-called *in situ* halo (main progenitor halo) with respect to the *ex situ* halo (accreted stellar system from outside) component. It is found that these halo components are spatially segregated, with *in situ* halo dominating the innermost regions of the halo space, and *ex situ* halo being deposited at larger Galactocentric distances in order of decreasing merger mass ratio. These properties are well summarized in their Figure 10: the *in situ* component shows a steep density profile below the transition radius, whereas the *ex situ* component beyond this radius provides a shallow slope having an outer boundary. This theoretical prediction may well reproduce the change of the halo density profile mentioned here, namely the steep profile in the inner halo probed by RR Lyrae, which were possibly formed *in situ*, and the shallow profile in the outer halo reported here using BHBs, which were originated from the *ex situ* component.

4. Prospects

In this contribution, we have reported the discovery of highly compelling UFD candidates and the distribution of BHB stars in the MW halo taken from the HSC-SSP data obtained through 2018 April. The HSC-SSP survey is currently on going and we plan to analyze much larger data obtained by the completion of the survey with a goal of $\sim 1,400$ deg^2. Also, further follow-up studies of UFD candidates and BHB stars discovered here are being made by combining spectroscopic and astrometric data available from both ground- and space-based telescopes.

The combination of Subaru and HSC allows us to conduct several science opportunities thanks to the superb image quality, depth and wide field of view. Indeed, we are

https://doi.org/10.1017/S1743921319008640 Published online by Cambridge University Press

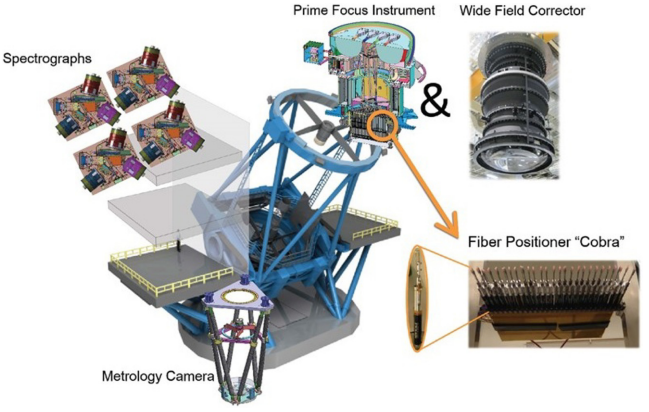

Figure 4. The Prime Focus Specrograph (PFS) system in the Subaru telescope (Credit: IPMU, the University of Tokyo).

now preparing new narrow-band filters for HSC, NB395 and NB430, focusing on the absorption regions of Ca HK at 395 nm and CH at 430 nm, respectively, to obtain the photometric information of [Fe/H] and [C/Fe] of stars. These HSC filters will especially be useful for photometrically searching for extremely metal-poor and/or pristine star candidates in the several regions of the MW halo and bulge.

A further revolution in this field of research will be expected based on efficient multi-object spectroscopy of wide and panoramic fields provided by the Subaru Prime Focus Spectrograph (PFS), which is now under construction. PFS is a spectrograph system with a fiber positioner system to be mounted at the prime focus of the Subaru telescope (Figure 4). The instrument allows simultaneous spectral observation of up to 2,400 astronomical targets in a wide field of view of 1.3 degree diameter at a time. With Subaru/PFS, we plan to measure the radial velocities and chemical abundances of large samples of stars in the MW disks and halo, in the MW satellite galaxies and in the M31 halo to infer the assembly histories of these galaxies and the structure of their dark matter halos (Takada *et al.* 2014).

References

Aihara, H., Arimoto, N., Armstrong, R., *et al.* 2018, *PASJ*, 70, S4
Bressan, A., Marigo, P., Girardi, L., *et al.* 2012, *MNRAS*, 427, 127
Cohen, J. G., Sesar, B., Banholzer, S. *et al.* 2017, *ApJ*, 849, 150
Deason, A. J., Belokurov, V., & Evans, N. W. 2011, *MNRAS*, 416, 2903
Dooley, G. A., Peter, A. H. G., Carlin, J. L. *et al.* 2017, *MNRAS*, 472, 1060
Einasto, J. 1965, *Trudy Inst. Astroz. Alma-Ata*, 5, 87
Fukushima, T., Chiba, M., Homma, D. *et al.* 2018, *PASJ*, 70, 69
Fukushima, T., Chiba, M., Tanaka, M. *et al.* 2019, *PASJ*, 71, 72
Hernitschek, N., Cohe, J. G., Rix, H.-W., *et al.* 2018, *ApJ*, 859, 31
Homma, D., Chiba, M., Okamoto, S., *et al.* 2018, *PASJ*, 70, S18
Homma, D., Chiba, M., Komiyama, Y., *et al.* 2019, *PASJ*, 71, 94
Kim, S. Y., Peter, A. H. G., & Hargis, J. R. 2018, *Phys. Rev. Letters*, 121, 21
Klypin, A., Kravtsov, A. V., Valenzuela, O., & Prada, F. 1999, *ApJ*, 522, 82
Lenz, D. D., Newberg, J., Rosner, R., *et al.* 1998, *ApJS*, 119, 121
Moore, B., Ghigna, S., Governato, F., Lake, G., Quinn, T., & Stadel, J. 1999, *ApJ (Letters)*, 524, L19
Newton, O., Cautun, M., Jenkins, A., *et al.* 2018, *MNRAS*, 479, 2853

https://doi.org/10.1017/S1743921319008640 Published online by Cambridge University Press

Rodriguez-Gomez, V., Pillepich, A., Sales, L. V., *et al.* 2016, *MNRAS*, 458, 2371
Springel, V. *et al.* 2008, *MNRAS*, 391. 1685
Takada, M., Ellis, R. S., Chiba, M. *et al.* 2014, *PASJ*, 66, R1
Tegmark, M. *et al.* 2004, *ApJ*, 606, 702
Thomas, G. A., McConnachie, A. W., Ibata, R. A., *et al.* 2018, *MNRAS*, 481, 5223
Vickers, J. J., Grebel, E. K., & Huxor, A. P. 2012, *AJ*, 143, 86
Watkins, L. L. *et al.* 2009, *MNRAS*, 398, 1757

https://doi.org/10.1017/S1743921319008640 Published online by Cambridge University Press